

Constraints on Population I/II neutron star–black hole binary formation by gravitational wave and radio observations

Tomoya Kinugawa^{(1)★}, Takashi Nakamura⁽²⁾, and Hiroyuki Nakano⁽³⁾

¹*Institute for Cosmic Ray Research, The University of Tokyo, Kashiwa, Chiba 277-8582, Japan*

²*Department of Physics, Graduate School of Science, Kyoto University, Kyoto 606-8502, Japan*

³*Faculty of Law, Ryukoku University, Kyoto 612-8577, Japan*

8 July 2022

ABSTRACT

Two neutron star (NS)–black hole (BH) binaries, GW200105 and GW200115 found in the LIGO/Virgo O3b run have smaller BH mass of 6–9 M_{\odot} which is consistent with Population I and II origin. Our population synthesis simulations using 10^6 Population I and II binaries with appropriate initial parameters show consistent binary mass, event rate, and no detection of radio pulsar (PSR) and BH binaries in our galaxy so far. Especially, we found possible progenitors of GW200105 and GW200115 which were formed at redshift $z = 0.15$ and $z = 1.6$ with binary mass of $(34M_{\odot}, 9.2M_{\odot})$ and $(23.7M_{\odot}, 10.6M_{\odot})$, respectively. The final masses of these binaries are $(6.85M_{\odot}, 2.14M_{\odot})$ and $(6.04M_{\odot}, 1.31M_{\odot})$ which look like $(9.0^{+1.7}_{-1.7}M_{\odot}, 1.91^{+0.33}_{-0.24}M_{\odot})$ of GW200105 and $(5.9^{+2.0}_{-2.5}M_{\odot}, 1.44^{+0.85}_{-0.29}M_{\odot})$ of GW200115, respectively. We also estimate that 2.68–19.7 PSR–BH binaries in our galaxy will be observed by SKA. The existence of NS–BHs in our galaxy can be confirmed in future SKA era. Using the GW observation of NS–BH mergers and the radio observation of PSR–BHs in future, we can get more severe constraints on the NS–BH formation process.

Key words: stars: population I/II, binaries: general relativity, gravitational waves, black hole mergers

1 INTRODUCTION

Two gravitational wave (GW) events of neutron star–black hole (NS–BH) coalescences, GW200105_162426 (abbreviated as GW200105) and GW200115_042309 (abbreviated as GW200115) were observed by the LIGO–Virgo detector network (Abbott et al. 2021). Table 1 is the summary of the events. Here, we present only the chirp mass $M_{\text{chirp}} = (m_1 m_2)^{3/5} / M^{1/5}$ (where $M = m_1 + m_2$), primary mass m_1 and secondary mass m_2 although the other parameters (spin etc.) have been estimated (e.g., an effective spin parameter defined with nondimensional spin parameters $(\chi_{1,z}$ and $\chi_{2,z})$ parallel to the orbital angular momentum, $\chi_{\text{eff}} = (m_1/M)\chi_{1,z} + (m_2/M)\chi_{2,z} = 0.00^{+0.13}_{-0.18}$ for GW200105 and $-0.15^{+0.24}_{-0.42}$ for GW200115 (The LIGO Scientific Collaboration et al. 2021b), see also Mandel & Smith (2021) for the BH spin of GW200115)¹. The NS–BH merger rate density (combined with analyses based on the two events, and including less significant search triggers) was estimated as $12\text{--}242\text{ yr}^{-1}\text{Gpc}^{-3}$. This estimation has been updated to $7.4\text{--}320\text{ yr}^{-1}\text{Gpc}^{-3}$ in The LIGO Scientific Collaboration et al.

(2021c) using the third Gravitational-wave Transient Catalog (GWTC-3) (The LIGO Scientific Collaboration et al. 2021b) (see also GWTC-2.1 The LIGO Scientific Collaboration et al. (2021a) and the fourth Open Gravitational-wave Catalog (4-OGC) (Nitz et al. 2021)).

After the announcement of Abbott et al. (2021), various works on the population of these binaries have appeared. The works includes studies on primordial BH (PBH) scenarios (Wang & Zhao 2022; Chen et al. 2021; Sasaki et al. 2021), isolated binary evolution scenarios (Shao & Li 2021; Broekgaarden & Berger 2021; Fragione et al. 2021) (see also Zhu (2021)), the mass distribution of NSs/BHs in GW events (Landry & Read 2021; Mandel & Broekgaarden 2021), hierarchical population inferences (Li et al. 2021), the tilt angle of the BH spin (Gompertz et al. 2021), prediction of short-duration gamma-ray bursts (Mandhai et al. 2021), highly unequal mass components (Antoniadis et al. 2021), quadruple-star systems (Vynatheya & Hammers 2021), the lower mass gap between NSs and BHs (Farah et al. 2021), dynamical interactions in low-mass young star clusters (Trani et al. 2021), and prediction on GW event rates (Wagg et al. 2021) observed by a space-based detector, LISA (Amaro-Seoane et al. 2017) (see also, Belczynski et al. (2021); Broekgaarden et al. (2021)). Mandel & Broekgaarden (2021) gave us a great summary on merger rates of compact object binaries, i.e., NS–NSs, BH–BHs and NS–BHs for GW observations and various formation

★ E-mail: kinugawa@icrr.u-tokyo.ac.jp

¹ To extract more detailed information from these binaries, we need multiband GW observations, i.e., ground-based and space-based detectors (see e.g., Liu & Shao (2021) as an extension of Isoyama et al. (2018); Nakano et al. (2021))

Table 1. Abbreviated event name, chirp mass M_{chirp} , primary mass m_1 and secondary mass m_2 in unit of the solar mass, M_{\odot} are from GWTC-3 (The LIGO Scientific Collaboration et al. 2021b). Each value is shown with the 90% credible interval.

Event name	M_{chirp}	m_1	m_2
GW200105	$3.42^{+0.08}_{-0.08}$	$9.0^{+1.7}_{-1.7}$	$1.91^{+0.33}_{-0.24}$
GW200115	$2.43^{+0.05}_{-0.07}$	$5.9^{+2.0}_{-2.5}$	$1.44^{+0.85}_{-0.29}$

channels. Using information from the NS-BH GW events and radio pulsar (PSR) surveys in which no PSR-BH has been observed, Pol et al. (2021) derived an upper limit (95% CL) of ~ 150 PSR-BHs in our galaxy with the beaming direction to the Earth. Chattopadhyay et al. (2021) calculated that 1–80 PSR-BHs are detectable by SKA observation.

In Kinugawa et al. (2017) (hereafter Paper I), we discussed the merger rate of Population (Pop) I, II and Pop III NS-BH binaries by using population synthesis Monte Carlo simulations, including the kick of NSs (Lyne & Lorimer 1994; Hansen & Phinney 1997) (see also Hobbs et al. (2005); Verbunt et al. (2017)). From Table 3 of Paper I, we found that the merger rates of Pop I, II and Pop III are $6.38\text{--}19.7\text{ yr}^{-1}\text{Gpc}^{-3}$, and $0.956\text{--}1.25\text{ yr}^{-1}\text{Gpc}^{-3}$, respectively. Therefore, the merger rate of Pop I and II NS-BHs in Paper I is consistent with the LIGO-Virgo result of $7.4\text{--}320\text{ yr}^{-1}\text{Gpc}^{-3}$ in The LIGO Scientific Collaboration et al. (2021c). This implies that there are many PSR-BHs made by Pop I and II binary systems. In this Letter, based on the analysis in Paper I, we also calculate the Pop I, II NS-BHs merger rate with other parameters and estimate the number of PSR-BHs detected by current and future observations.

2 ANALYSIS

Theoretically NS-BH binaries can be formed in a certain evolution of binary stars. BH is usually formed first and next is NS because BH is usually formed from more massive star with shorter evolution time than the progenitor of NS. This means that some of them can be observed as a binary radio PSR with BH. However, no such object has been observed so far. This situation of no observed radio counter object of NS-BH binary is allowed if the expected number of NS-BH radio PSRs observed by existing radio telescopes is smaller than or compatible with the order of unity.

2.1 Population synthesis method

In Paper I, we performed population synthesis Monte Carlo simulations of Pop I, II and III binary stars using 10^6 binaries calculated by a modified BSE code (Hurley et al. 2002; Kinugawa et al. 2014; Kinugawa et al. 2016) for each given metallicity of $Z = Z_{\odot}$, $10^{-0.5}Z_{\odot}$, $10^{-1}Z_{\odot}$, $10^{-1.5}Z_{\odot}$, $10^{-2}Z_{\odot}$ and $Z = 0$ (i.e., Pop III stars) where Z_{\odot} is the metallicity of the Sun. We used the Madau star-formation rate (SFR) (Madau & Dickinson 2014), and calculated the metallicity evolution using the galaxy mass-metallicity relation evaluated by simulation (Ma et al. 2016) and the galaxy mass distribution fitted by the Shechter function (Fontana et al.

Table 2. Parameters for eight models.

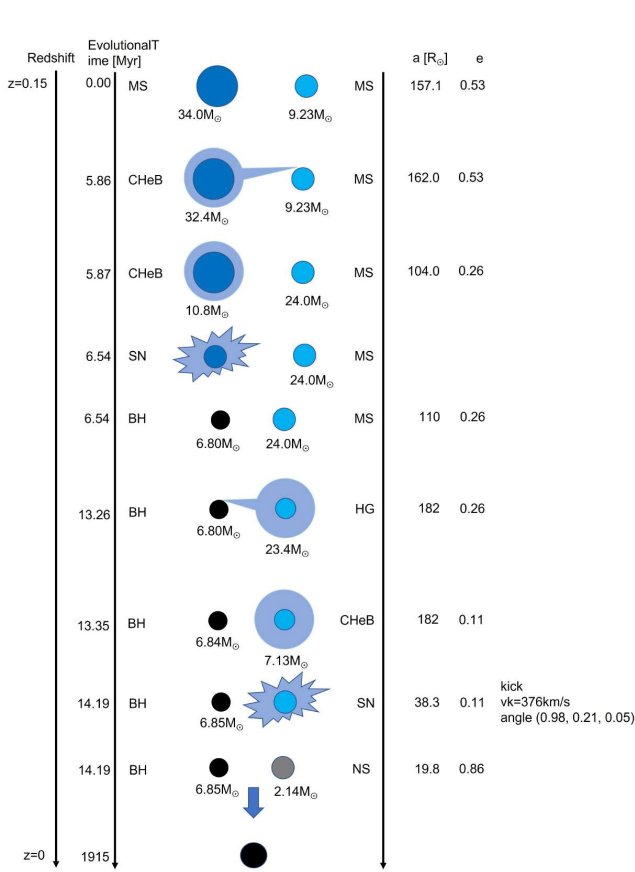
model	σ_k	$\alpha\lambda$	β	BH kick
Standard	265 km/s	1	0	off
$\sigma_k = 500\text{ km/s}$	500 km/s	1	0	off
$\alpha\lambda = 0.1$	265 km/s	0.1	0	off
$\alpha\lambda = 0.5$	265 km/s	0.5	0	off
$\alpha\lambda = 10$	265 km/s	10	0	off
$\beta = 0.1$	265 km/s	1	0.1	off
$\beta = 0.5$	265 km/s	1	0.5	off
BH kick	265 km/s	1	0	on

2006). We assumed the metallicity Z is changed as a function of redshift z taking the intermediate value in log scale such as $Z = 10^{-1.75}Z_{\odot}$ ($z = 6.745$), $10^{-1.25}Z_{\odot}$ ($z = 5.168$), $10^{-0.75}Z_{\odot}$ ($z = 2.528$), and $10^{-0.25}Z_{\odot}$ ($z = 0.096$). We choose the binary initial conditions, i.e., the primary mass M_1 , the mass ratio $q = M_2/M_1$, the separation a , and the eccentricity e when the binary is born. We adopt the Salpeter initial mass function (IMF) ($5M_{\odot} < M_1 < 140M_{\odot}$), the flat initial mass ratio function ($0.1M_{\odot}/M_1 < q < 1$), the logflat initial separation function ($a_{\text{min}} < a < 10^6 R_{\odot}$), and the thermal initial eccentricity distribution function ($0 < e < 1$) for Pop I, II binaries. On the other hand, we adopt the flat IMF and the different minimum mass ($10M_{\odot}$) for Pop III stars. We adopt in the simulation that when NS is formed it gets kick velocity of Maxwellian shaped absolute value with random direction. We adopt two values of velocity dispersion of the kick velocity σ_k of 265 km/s and 500 km/s. The former value of the kick velocity is that of the observed single PSRs (Hobbs et al. 2005) and the latter is that of young PSRs (Verbunt et al. 2017).

In this Letter, we also calculate the Pop I, II NS-BH evolution with other binary parameters, i.e., the common envelope parameters $\alpha\lambda$, and the mass loss fraction β during the Roche lobe over flow (Hurley et al. 2002; Kinugawa et al. 2014; Kinugawa et al. 2016). In Paper I, we assumed $\alpha\lambda = 1$ and $\beta = 0$ and no natal kick for BH formations. Here, we also consider the cases of $\alpha\lambda = 0.1, 0.5, 10, \beta = 0.1, 0.5$ and the BH natal kick. Then, each model is characterized by the values of σ_k , $\alpha\lambda$, β , and the switch of the BH natal kick. For simplicity, we treat only eight models defined by the values of σ_k , $\alpha\lambda$, β , and the switch of the BH natal kick (see Table 2). We consider 1) two models with different values of $\sigma_k = 265\text{ km/s}$ or 500 km/s , but the same values of $\alpha\lambda = 1$ and $\beta = 0$ with no BH natal kick, 2) three models with different values of $\alpha\lambda = 0.1, 0.5$ and 10 , but the same values of $\sigma_k = 265\text{ km/s}$ and $\beta = 0$ with no BH natal kick, 3) two models with $\beta = 0.1$ and 0.5 , but $\alpha\lambda = 1$ and $\sigma_k = 265\text{ km/s}$ with no BH natal kick, and 4) the BH natal kick model with $\sigma_k = 265\text{ km/s}$, $\alpha\lambda = 1$ and $\beta = 0$. Table 3 shows the merger rates of NS-BHs at the present day for each model. We show two examples from our simulation for $\sigma_k = 265\text{ km/s}$, $\alpha\lambda = 1$ and $\beta = 0$ with no BH natal kick: the first one shown in Figure 1 is a NS-BH binary formed at redshift $z = 0.15$ with $m_1 = 6.85M_{\odot}$ and $m_2 = 2.14M_{\odot}$ which looks like GW200105, while the second one shown in Figure 2 is that of a NS-BH binary formed at $z = 1.6$ with $m_1 = 6.04M_{\odot}$ and $m_2 = 1.31M_{\odot}$ which looks like GW200115. These examples are made from binaries with $Z = 10^{-0.5}Z_{\odot}$ which were born within a range

Table 3. Pop I, II NS-BH merger rate at the present day for each model.

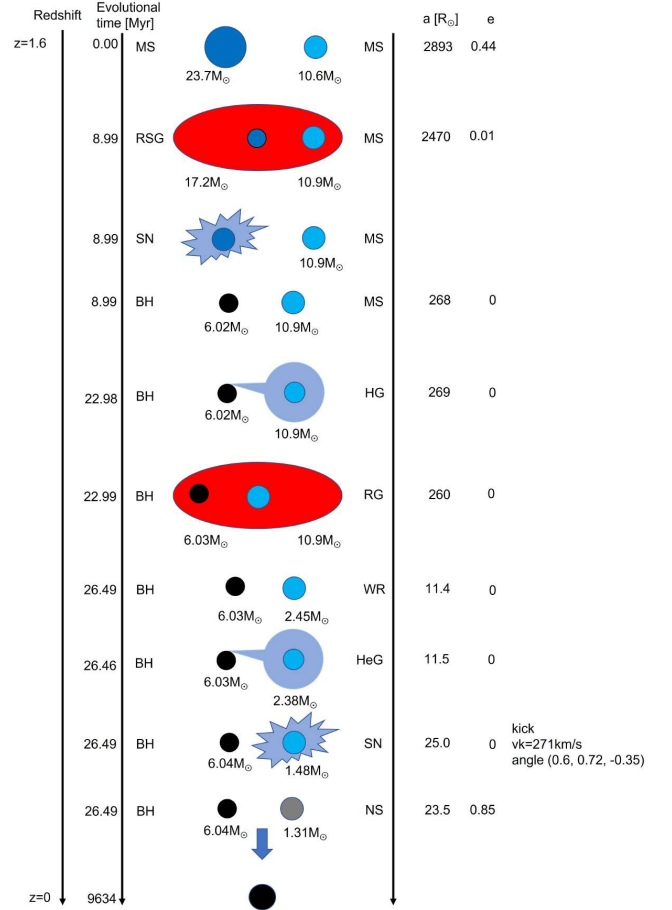
	Standard	$\sigma_k = 500$ km/s	$\alpha\lambda = 0.1$	$\alpha\lambda = 0.5$	$\alpha\lambda = 10$	$\beta = 0.1$	$\beta = 0.5$	BH kick
NS-BH merger rate [$\text{Gpc}^{-3} \text{ yr}^{-1}$]	19.7	6.38	19.1	23.2	1.07	18.0	19.0	5.78


Figure 1. The formation of a NS-BH with $m_1 = 6.85 M_\odot$ and $m_2 = 2.14 M_\odot$ which looks like GW200105 shown in Table 1. The pulsar kick velocity is 376 km/s with kick angle (0.98, 0.21, 0.05) where the kick angle is defined in Figure A1 of Hurley et al. (2002). MS, ChHeB SN, BH, HG, and NS means a main sequence phase, a core Helium burning, a supernova, a black hole, a Hertzsprung gap phase, and a neutron star, respectively.

of $z = 0.1$ – 2.5 . Note here that binaries with $Z = 10^{-0.5} Z_\odot$ dominate the merger rate of NS-BHs at $z = 0$ as shown in Figures 2 and 3 of Paper I.

2.2 detectability of Pulsar- black hole binaries

Table 4 of this Letter shows metallicity dependence on numbers of NS-BH formation in 10^6 Monte Carlo simulations. The numbers in parenthesis are NS-BHs which merge within the Hubble time. We treat two velocity dispersion models of the kick velocity of $\sigma_k = 265$ km/s, and $\sigma_k = 500$ km/s. Figure 3 shows the NS-BH merger rate densities for each model. The peak of chirp mass distribution of detectable NS-BHs is around 2 – $3 M_\odot$, which is consistent with the observa-


Figure 2. The formation of a NS-BH with $m_1 = 6.04 M_\odot$ and $m_2 = 1.31 M_\odot$ which looks like GW200115 shown in Table 1. The pulsar kick velocity is 271 km/s with kick angle (0.6, 0.72, -0.35) where the kick angle is defined in Figure A1 of Hurley et al. (2002). RSG, RG, WR, and HeG mean a red super giant, a red giant, a Wolf-Rayet star, and a Helium giant, respectively.

tion of GW200105 and GW200115 since their chirp mass are $3.42 M_\odot$ and $2.43 M_\odot$, respectively.

Figures 1 and 2 suggest that PSR-BH binaries should be observed in a certain time of the universe for each NS-BH binary formed in our scenario. The typical maximum age of observable radio PSRs is $\sim 5 \times 10^7$ yrs from the PSR death line for the magnetic field strength of $\sim 10^{12}$ G which is typical for newborn PSRs and PSRs in high mass X-ray binaries (HMXBs) (Enoto et al. 2019). We first estimate the number of NS-BHs formed from 5×10^7 yrs ago up to now in our galaxy. Using the first column of Table 4 for $Z = Z_\odot$, we obtain that the fraction of NS-BH binary is $(0.2$ – $2.03) \times 10^{-4}$.

The star formation rate of our galaxy at present is $1.65 M_\odot/\text{yr}$ (Licquia & Newman 2015). Here, we use the generally accepted Salpeter-like initial mass function of the form

Table 4. Metallicity dependence on numbers of NS-BH formation in 10^6 Monte Carlo simulations. The numbers in parentheses are NS-BHs which merge within the Hubble time. We treat five models with kick velocity of $\sigma_k = 265$ km/s and $\sigma_k = 500$ km/s, $\alpha\lambda = 0.1$ and 10, and $\beta = 0.5$.

Z	Z_\odot	$10^{-0.5}Z_\odot$	$10^{-1}Z_\odot$	$10^{-1.5}Z_\odot$	$10^{-2}Z_\odot$
NS-BH [Standard]	147 (15)	598 (191)	1295 (524)	1686 (755)	1896 (862)
NS-BH [$\sigma_k = 500$ km/s]	32 (2)	169 (67)	416 (213)	576 (377)	617 (401)
NS-BH [$\alpha\lambda = 0.1$]	128 (48)	362 (148)	1312 (518)	1941 (845)	1932 (840)
NS-BH [$\alpha\lambda = 0.5$]	203 (29)	651 (283)	1428 (665)	1724 (790)	1907 (755)
NS-BH [$\alpha\lambda = 10$]	20 (0)	119 (14)	383 (22)	928 (100)	1271 (200)
NS-BH [$\beta = 0.1$]	60 (9)	637 (191)	1443 (556)	1938 (704)	2242 (849)
NS-BH [$\beta = 0.5$]	65 (5)	627 (190)	1404 (547)	1828 (720)	2060 (842)
NS-BH [BH kick]	44 (16)	124 (52)	437 (262)	782 (482)	935 (503)

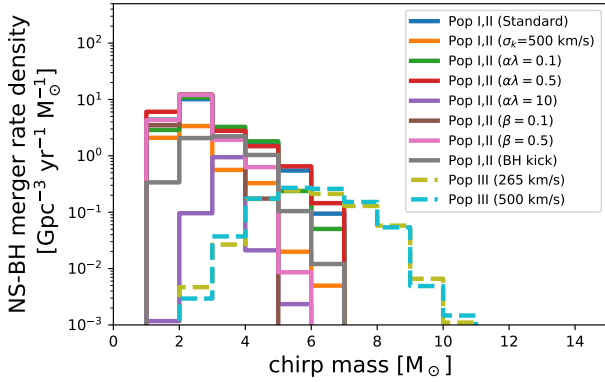


Figure 3. Chirp mass distributions of detectable NS-BHs at $z = 0$. The solid lines show the cases of Pop I, II NS-BH merger rates for each model, respectively. The dashed lines show the merger rates of Pop III NS-BHs from Paper I, respectively.

$$\phi(m) = Cm^{-2.3}, \quad (1)$$

which is appropriate for $m > 0.5 M_\odot$ (Kroupa & Jerabkova 2019). Since the total mass of the new born stars in 5×10^7 yrs is $8.3 \times 10^7 M_\odot$, we have the equality

$$\int_{0.5M_\odot}^{\infty} m\phi(m)dm = 8.3 \times 10^7 M_\odot. \quad (2)$$

Then, the constant C is determined as

$$C = 1.9 \times 10^7 M_\odot^{1.3}. \quad (3)$$

In the calculation of Paper I, we have considered only stars with mass larger than $5 M_\odot$ because we are interested in NS-BHs. Then, the total number of stars with mass larger than $5 M_\odot$ is given by

$$\int_{5M_\odot}^{\infty} \phi(m)dm = 2.0 \times 10^6. \quad (4)$$

Assuming here that 50% of the stellar systems are binaries, the number of binaries is 6.7×10^5 . Under this assumption, the number of the Pop I binary stars which evolve to PSR-BHs become $(0.2-2.03) \times 10^{-4} \times 6.7 \times 10^5 = 13.4-136$ (see Table 5).

Now PSRs are beaming so that only the fraction of ~ 0.2 can be observed (Pol et al. 2019) (see also Kim et al. (2015)).

While at present all the PSRs in our galaxy are not observed but only 10% (Lorimer 2008) or so (see also a recent review Combes (2021)) due to the sensitivity of radio telescopes at present, in the SKA era almost all the active radio PSRs in our galaxy can be observed (Keane et al. 2015). Thus, the expected number of active NS-BHs in our galaxy found in radio band at present is 0.268–2.72. This expected number for NS-BHs is marginal for detection which depends on the direction of magnetic field of the pulsar, the radio power, the distance to the pulsar and so on. Thus, the current no observation of NS-BH radio PSRs is more or less consistent.

In relation to this marginal situation, it would be interesting to point out the observation history of PSR J1740-3052 which was found in 2001 (Stairs et al. 2001). This binary PSR has a PSR period of 0.57 sec and the characteristic age of 3.5×10^5 yrs with the orbital period of 231 days and the mass function of $8.7 M_\odot$. Thus the companion mass exceeds $11 M_\odot$ so that it was not possible to rule out a BH companion in 2001 when this binary was found. At this time PSR J1740-3052 could be a NS-BH binary formed in our above scenario for example. After 11 years from the discovery of PSR J1740-3052, Madsen et al. (2012) found the main sequence star companion, and concluded that PSR J1740-3052 is not a NS-BH binary. However, because the expected number of observable NS-BH binaries in future SKA era is 2.68–27.2, the existence of NS-BH binaries in our galaxy can be confirmed in future.

Figure 4 shows the BH mass distributions of detectable NS-BH mergers at $z = 0$ (the left panel) and galactic PSR-BHs (the right panel). Since the galactic PSR-BHs are made by Pop I ($Z = Z_\odot$) stars, the BH masses of PSR-BHs are typically lower than those of NS-BHs which are detectable by the GWs.

Figure 5 shows the merger rates of NS-BHs and the numbers of galactic PSR-BHs for each model. The blue shaded region shows the constraint of the NS-BH merger rate of LIGO-Virgo result of $7.4-320 \text{ yr}^{-1} \text{ Gpc}^{-3}$. The orange shaded region shows the constraint where the number of detectable galactic PSR-BHs by the present radio observation is less than 1. Here, we define the upper limit of the number of detectable galactic PSR-BHs by the present radio observation is 1 because there is no observation of PSR-BH now. When the above upper limit becomes reality, we can say the followings. The $\beta = 0.1$ model and the $\beta = 0.5$ model satisfy these constraints. The standard model, the $\alpha\lambda = 0.1$ model, and the $\alpha\lambda = 0.5$ model are consistent with the NS-BH merger rate,

Table 5. The numbers of galactic PSR-BHs for each model. The total numbers of galactic PSR-BHs and the numbers of observable PSR-BHs by future SKA observation for each model are shown out of and in parentheses, respectively.

	Standard	$\sigma_k = 500$ km/s	$\alpha\lambda = 0.1$	$\alpha\lambda = 0.5$	$\alpha\lambda = 10$	$\beta = 0.1$	$\beta = 0.5$	BH kick
PSR-BHs	98.5 (19.7)	21.4 (4.29)	85.8 (17.2)	136 (27.2)	13.4 (2.68)	40.2 (8.04)	43.6 (8.71)	29.5 (5.90)

but not consistent with the number of detectable PSR-BHs by the present radio observation slightly. On the other hand, the $\sigma_k = 500$ km/s model and the BH kick model are consistent with the number of detectable PSR-BHs by the present radio observation, but not consistent with the NS-BH merger rate slightly. In the case of the $\alpha\lambda = 10$ model, although it satisfies the constraint of the number of detectable PSR-BHs, the NS-BH merger rate of this model is about 10 times less than the lower limit of the LIGO result.

At present the blue and orange shaded regions in Figure 5 are very large because of small number of NS-BHs observed by GW and none of PSR-BH observed by radio. However, they will increase so that we can get severe constraints on the possible theoretical model in future.

3 DISCUSSION

Some of NS-BHs which have a radio emission can be observed as PSR-BHs. Our calculation shows that the SKA will detect 2.68–19.7 PSR-BHs in our galaxy. We can check the consistency of the field binary model not only with the merger rate of NS-BHs, but also with the PSR-BH observations by future SKA. This can give a stronger constraint than Figure 5. Since the SKA will find only young NS-BHs because the PSR lifetime is only $\sim 5 \times 10^7$ yrs, the origin of such NS-BHs will be confirmed as Pop I stars. The maximum BH mass of Pop I PSR-BHs is $\lesssim 20 M_\odot$ (see Figure 4). On the other hand, NS-BHs which are detected by GW observations are possibly the summation of each metallicity of Pop I, Pop II and Pop III. The maximum BH mass of these NS-BHs is much more than $20 M_\odot$ (see Figure 4). Thus, the comparison of the BH mass distribution of NS-BH binaries detected by GW observations with the BH mass distribution of PSR-BHs detected by the SKA might show the dependence of BH mass on the metallicity.

In our calculation, we have ignored the life prolongation of the spin due to accretion from a companion star like millisecond PSRs. Here, $\sim 90\%$ of NS-BHs are formed as BH1st–NS2nd where BH1st–NS2nd means that the primary star which is initially more massive than the companion star evolves to the BH first, and the secondary star evolves to the NS next. In this case, accretion onto the NS does not occur. On the other hand, $\sim 10\%$ of NS-BHs are formed as NS1st–BH2nd which means that the primary star evolves to the NS first, and the secondary star evolves to the BH next. In this case, progenitors of NS1st–BH2nd evolve via HMXBs so that accretion onto the NS can occur. However the spin up due to accretion onto the NSs in HMXBs does not occur in general. The magnetic field strength of the NSs in HMXBs is typically so large ($\sim 10^{12}$ G) (Enoto et al. 2019) that the matter cannot accrete directly onto the NS surface in the disc plane, but rather forms a funnel flow onto the magnetic poles because it

is constrained to follow the magnetic field lines (e.g. Pringle & Rees 1972). Thus, the PSR lifetime of NS1st–BH2nd has been treated similar to that of BH1st–NS2nd in this Letter.

ACKNOWLEDGMENT

We thank the anonymous referee and Wataru Ishizaki for useful comments. T. K. acknowledges support from the University of Tokyo Young Excellent Researcher program and from JSPS KAKENHI Grant Number JP21K13915. H. N. acknowledges support from JSPS KAKENHI Grant Numbers JP21K03582, JP21H01082 and JP17H06358.

DATA AVAILABILITY

Results will be shared on reasonable request to corresponding author.

REFERENCES

- Abbott R., et al., 2021, *Astrophys. J. Lett.*, 915, L5
Amaro-Seoane P., et al., 2017, arXiv e-prints, p. [arXiv:1702.00786](#)
Antoniadis J., et al., 2021, arXiv e-prints, p. [arXiv:2110.01393](#)
Belczynski K., et al., 2021, arXiv e-prints, p. [arXiv:2108.10885](#)
Broekgaarden F. S., Berger E., 2021, *ApJ*, 920, L13
Broekgaarden F. S., Berger E., Stevenson S., Justham S., Mandel I., Chruślińska M., 2021, arXiv e-prints, p. [arXiv:2112.05763](#)
Chattopadhyay D., Stevenson S., Hurley J. R., Bailes M., Broekgaarden F., 2021, *MNRAS*, 504, 3682
Chen Z.-C., Yuan C., Huang Q.-G., 2021, arXiv e-prints, p. [arXiv:2108.11740](#)
Combes F., 2021, arXiv e-prints, p. [arXiv:2107.03915](#)
Enoto T., Kisaka S., Shibata S., 2019, *Reports on Progress in Physics*, 82, 106901
Farah A. M., Fishbach M., Essick R., Holz D. E., Galadage S., 2021, arXiv e-prints, p. [arXiv:2111.03498](#)
Fontana A., et al., 2006, *A&A*, 459, 745
Fragione G., Loeb A., Rasio F. A., 2021, *ApJ*, 918, L38
Gompertz B. P., Nicholl M., Schmidt P., Pratten G., Vecchio A., 2021, arXiv e-prints, p. [arXiv:2108.10184](#)
Hansen B. M. S., Phinney E. S., 1997, *MNRAS*, 291, 569
Hobbs G., Lorimer D. R., Lyne A. G., Kramer M., 2005, *MNRAS*, 360, 974
Hurley J. R., Tout C. A., Pols O. R., 2002, *MNRAS*, 329, 897
Isoyama S., Nakano H., Nakamura T., 2018, *Progress of Theoretical and Experimental Physics*, 2018, 073E01
Keane E., et al., 2015, in *Advancing Astrophysics with the Square Kilometre Array (AASKA14)*. p. 40 ([arXiv:1501.00056](#))
Kim C., Perera B. B. P., McLaughlin M. A., 2015, *MNRAS*, 448, 928
Kinugawa T., Inayoshi K., Hotokezaka K., Nakauchi D., Nakamura T., 2014, *MNRAS*, 442, 2963
Kinugawa T., Miyamoto A., Kanda N., Nakamura T., 2016, *MNRAS*, 456, 1093

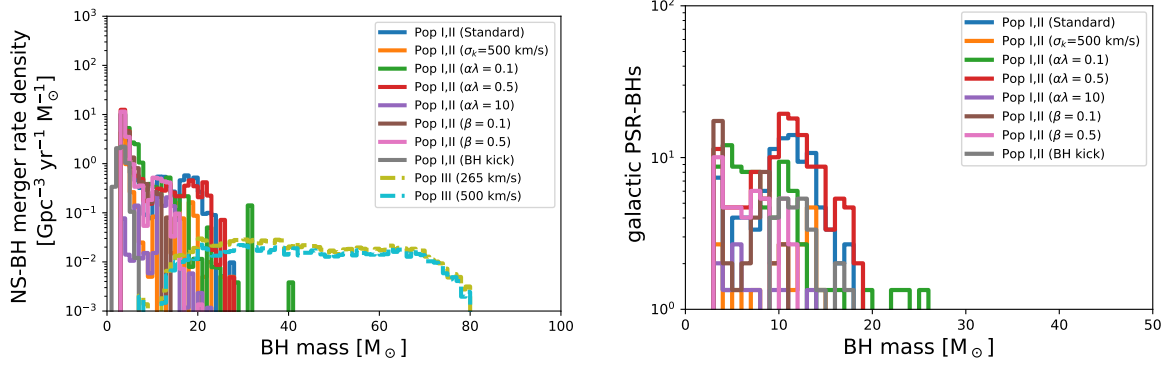


Figure 4. The left panel shows BH mass distributions of detectable NS-BHs at $z = 0$. The solid lines are the cases of Pop I,II NS-BHs for each model. The dashed lines are the case of Pop III NS-BHs. The right panel shows the BH mass distributions of galactic PSR-BHs for each model.

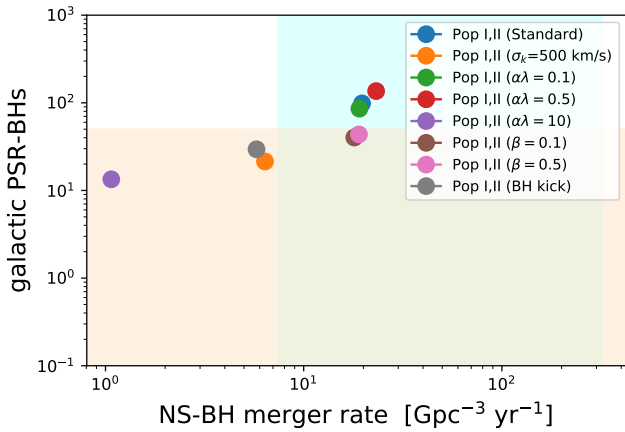


Figure 5. The merger rates of NS-BHs and the numbers of galactic PSR-BHs for each model. The blue shaded region shows the constraint of the NS-BH merger rate $7.4\text{--}320\text{ yr}^{-1}\text{Gpc}^{-3}$. The orange shaded region shows the constraint where the number of detectable galactic PSR-BHs by the present radio observation is less than 1.

Kinugawa T., Nakamura T., Nakano H., 2017, *Progress of Theoretical and Experimental Physics*, 2017, 021E01
 Kroupa P., Jerabkova T., 2019, *Nature Astronomy*, 3, 482
 Landry P., Read J. S., 2021, *ApJ*, 921, L25
 Li Y.-J., Tang S.-P., Wang Y.-Z., Han M.-Z., Yuan Q., Fan Y.-Z., Wei D.-M., 2021, *ApJ*, 923, 97
 Licquia T. C., Newman J. A., 2015, *ApJ*, 806, 96
 Liu C., Shao L., 2021, arXiv e-prints, p. arXiv:2108.08490
 Lorimer D. R., 2008, *Living Reviews in Relativity*, 11, 8
 Lyne A. G., Lorimer D. R., 1994, *Nature*, 369, 127
 Ma X., Hopkins P. F., Faucher-Giguère C.-A., Zolman N., Muratov A. L., Kereš D., Quataert E., 2016, *MNRAS*, 456, 2140
 Madau P., Dickinson M., 2014, *ARA&A*, 52, 415
 Madsen E. C., et al., 2012, *MNRAS*, 425, 2378
 Mandel I., Broekgaarden F. S., 2021, arXiv e-prints, p. arXiv:2107.14239
 Mandel I., Smith R. J. E., 2021, *ApJ*, 922, L14
 Mandhai S., Lamb G. P., Tanvir N. R., Bray J., Nixon C. J., Eyles-Ferris R. A. J., Levan A. J., Gompertz B. P., 2021, arXiv e-prints, p. arXiv:2109.09714
 Nakano H., Fujita R., Isoyama S., Sago N., 2021, *Universe*, 7, 53
 Nitz A. H., Kumar S., Wang Y.-F., Kastha S., Wu S., Schäfer M., Dhurkunde R., Capano C. D., 2021, arXiv e-prints, p. arXiv:2112.06878

Pol N., McLaughlin M., Lorimer D. R., 2019, *ApJ*, 870, 71
 Pol N., McLaughlin M., Lorimer D., 2021, arXiv e-prints, p. arXiv:2109.04512
 Pringle J. E., Rees M. J., 1972, *A&A*, 21, 1
 Sasaki M., Takhistov V., Vardanyan V., Zhang Y.-l., 2021, arXiv e-prints, p. arXiv:2110.09509
 Shao Y., Li X.-D., 2021, *ApJ*, 920, 81
 Stairs I. H., et al., 2001, *MNRAS*, 325, 979
 The LIGO Scientific Collaboration et al., 2021a, arXiv e-prints, p. arXiv:2108.01045
 The LIGO Scientific Collaboration et al., 2021b, arXiv e-prints, p. arXiv:2111.03606
 The LIGO Scientific Collaboration The Virgo Collaboration The KAGRA Scientific Collaboration 2021c, arXiv e-prints, p. arXiv:2111.03634
 Trani A. A., Rastello S., Di Carlo U. N., Santoliquido F., Tanikawa A., Mapelli M., 2021, arXiv e-prints, p. arXiv:2111.06388
 Verbunt F., Igoshev A., Cator E., 2017, *A&A*, 608, A57
 Vynatheya P., Hamers A. S., 2021, arXiv e-prints, p. arXiv:2110.14680
 Wagg T., Broekgaarden F. S., de Mink S. E., van Son L. A. C., Frankel N., Justham S., 2021, arXiv e-prints, p. arXiv:2111.13704
 Wang S., Zhao Z.-C., 2022, *Eur. Phys. J. C*, 82, 9
 Zhu X.-J., 2021, *ApJ*, 920, L20